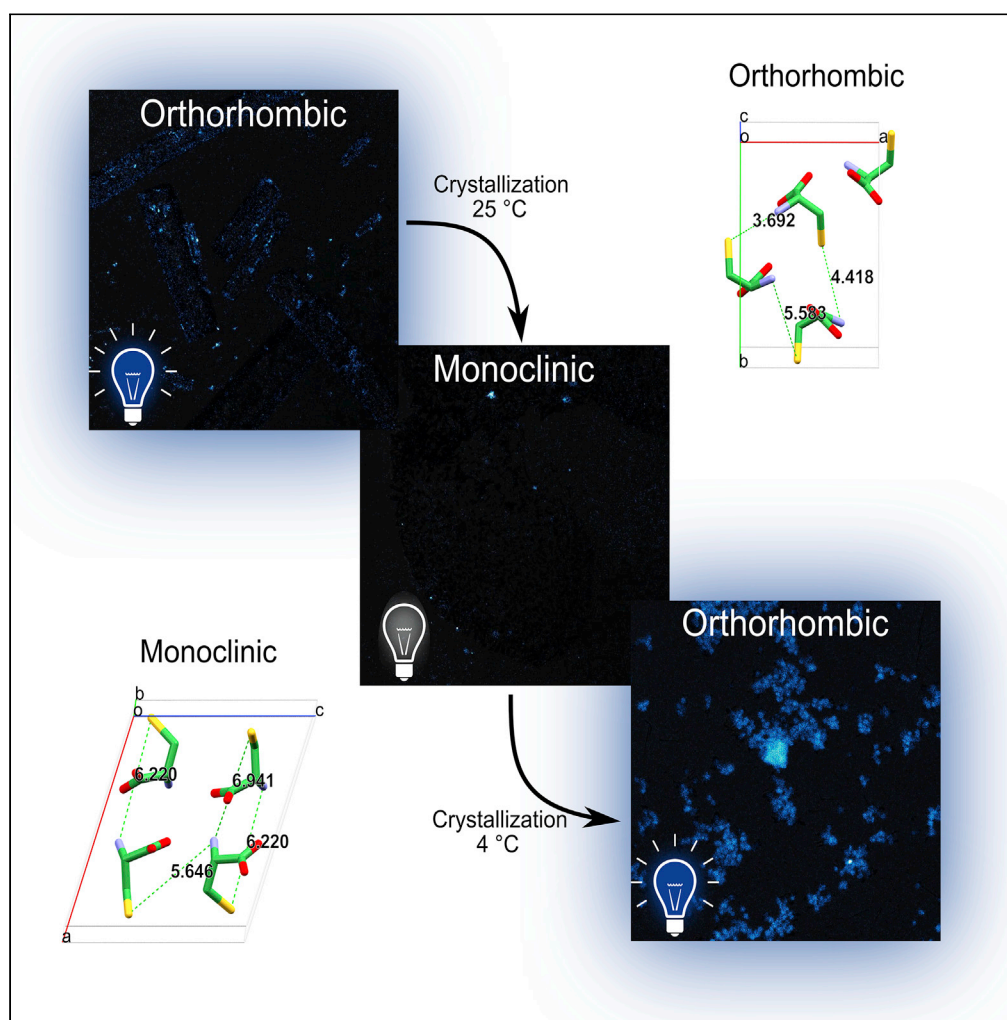


Article

On-off transition and ultrafast decay of amino acid luminescence driven by modulation of supramolecular packing



Zohar A. Arnon,
Topaz Kreiser,
Boris Yakimov, ...,
Evgeny Shirshin,
Davide Levy, Ehud
Gazit

ehudga@tauex.tau.ac.il

Highlights

Systematic
autofluorescence
characterization of all
coded amino acids was
performed

Lysine, a non-aromatic
amino acid, exhibited the
highest fluorescent signal

Reversible transition
between cysteine crystals
determines on-off
autofluorescence

Ultrafast lifetime decay
shown experimentally,
confirming governing role
in emission

Arnon et al., iScience 24,
102695
July 23, 2021 © 2021
[https://doi.org/10.1016/
j.isci.2021.102695](https://doi.org/10.1016/j.isci.2021.102695)

Article

On-off transition and ultrafast decay of amino acid luminescence driven by modulation of supramolecular packing

Zohar A. Arnon,^{1,9} Topaz Kreiser,^{1,9} Boris Yakimov,² Noam Brown,¹ Ruth Aizen,¹ Shira Shaham-Niv,³ Pandeewar Makam,¹ Muhammad Nawaz Qaisrani,⁴ Emiliano Poli,⁴ Antonella Ruggiero,⁵ Inna Slutsky,⁵ Ali Hassanali,⁴ Evgeny Shirshin,^{2,6} Davide Levy,⁷ and Ehud Gazit^{1,8,10,*}

SUMMARY

Luminescence of biomolecules in the visible range of the spectrum has been experimentally observed upon aggregation, contrary to their monomeric state. However, the physical basis for this phenomenon is still elusive. Here, we systematically examine all coded amino acids to provide non-biased empirical insights. Several amino acids, including non-aromatic, show intense visible luminescence. Lysine crystals display the highest signal, whereas the very chemically similar non-coded ornithine does not, implying a role for molecular packing rather than the chemical characteristics. Furthermore, cysteine shows luminescence that is indeed crystal packing dependent as repeated rearrangements between two crystal structures result in a reversible on-off optical transition. In addition, ultrafast lifetime decay is experimentally validated, corroborating a recently raised hypothesis regarding the governing role of $n\pi^*$ states in the emission formation. Collectively, our study supports that electronic interactions between non-fluorescent, non-absorbing molecules at the monomeric state may result in reversible optically active states by the formation of supramolecular fluorophores.

INTRODUCTION

In nature, proteins and peptides offer a broad range of characteristics and attributes, which provide an extensive variety of mechanical, electrical, and optical properties. These are often derived from the physicochemical properties of the amino acid building blocks that constitute the proteinaceous polymer. In addition to the amino acid content, the arrangement of the protein in its environment, i.e., secondary, tertiary, and quaternary structure, can dramatically influence the resulting physical properties. This arrangement is affected by factors such as the solvent, temperature, and ionic strength. Recently, several studies described the intrinsic luminescence in the visible range of protein assemblies, whereas the monomeric protein in solution is not luminescent (Bhattacharya et al., 2017; Pinotsi et al., 2016). Consistently, it is now evident that some amyloids, once assembled, exhibit fluorescence that is not demonstrated in the monomeric state in solution (Ardon et al., 2017; Chan et al., 2013; Del Mercato et al., 2007; Pinotsi et al., 2013).

Monomeric amino acids were subjected to extensive research over the years. Recently, a great emphasis was given to the ability of amino acids to serve as building blocks for the formation of various supramolecular assemblies with attractive features (Guerin et al., 2018; Ji et al., 2019; Makam et al., 2019). It was shown that single amino acids in their aggregated form can also produce a fluorescent signal, which is not evident in the monomeric state (Babar and Sarkar, 2017; Banerjee et al., 2020; Niyangoda et al., 2017; Shaham-Niv et al., 2018). Numerous observations suggest that the optical phenomenon of aggregation-induced intrinsic fluorescence is broader than originally speculated, as it also applies to many other metabolites and nucleic acids (Arnon et al., 2019; Berger et al., 2015; Chen et al., 2018; Lakowicz et al., 2001; Stephens et al., 2020; Zou et al., 2002). Circumstantial evidence and argumentation suggested that supramolecular packing is important. It was suggested that the hydrogen bonds and, in specific cases, the aromatic stacking, can underlie these optical properties (Jong et al., 2019; Pinotsi et al., 2016). Yet, other views have suggested impurities and oxidation as alternative mechanisms, ascribing no significant role to the molecular

¹Department of Molecular Microbiology and Biotechnology, George S. Wise Faculty of Life Sciences, Tel Aviv University, Tel Aviv 6997801, Israel

²Faculty of Physics, M.V. Lomonosov Moscow State University, Moscow 119991 Russia

³BLAVATNIK CENTER for Drug Discovery, Metabolite Medicine Division, Tel Aviv University, Tel Aviv 6997801, Israel

⁴International Centre for Theoretical Physics, Strada Costiera, 11, 34151 Trieste, Italy

⁵Department of Physiology and Pharmacology, Sackler Faculty of Medicine, Tel Aviv University, Tel Aviv University, 6997801 Tel Aviv, Israel

⁶Institute for Regenerative Medicine, I.M. Sechenov Moscow State Medical University, 119991 Moscow, Russia

⁷X-Ray Diffraction Lab, Wolfson Applied Materials Research Centre, Tel Aviv University, Tel Aviv 6997801, Israel

⁸Department of Materials Science and Engineering Iby and Aladar Fleischman Faculty of Engineering, Tel Aviv University, Tel Aviv 6997801, Israel

⁹These authors contributed equally

¹⁰Lead contact

*Correspondence: ehudga@tauex.tau.ac.il
<https://doi.org/10.1016/j.isci.2021.102695>



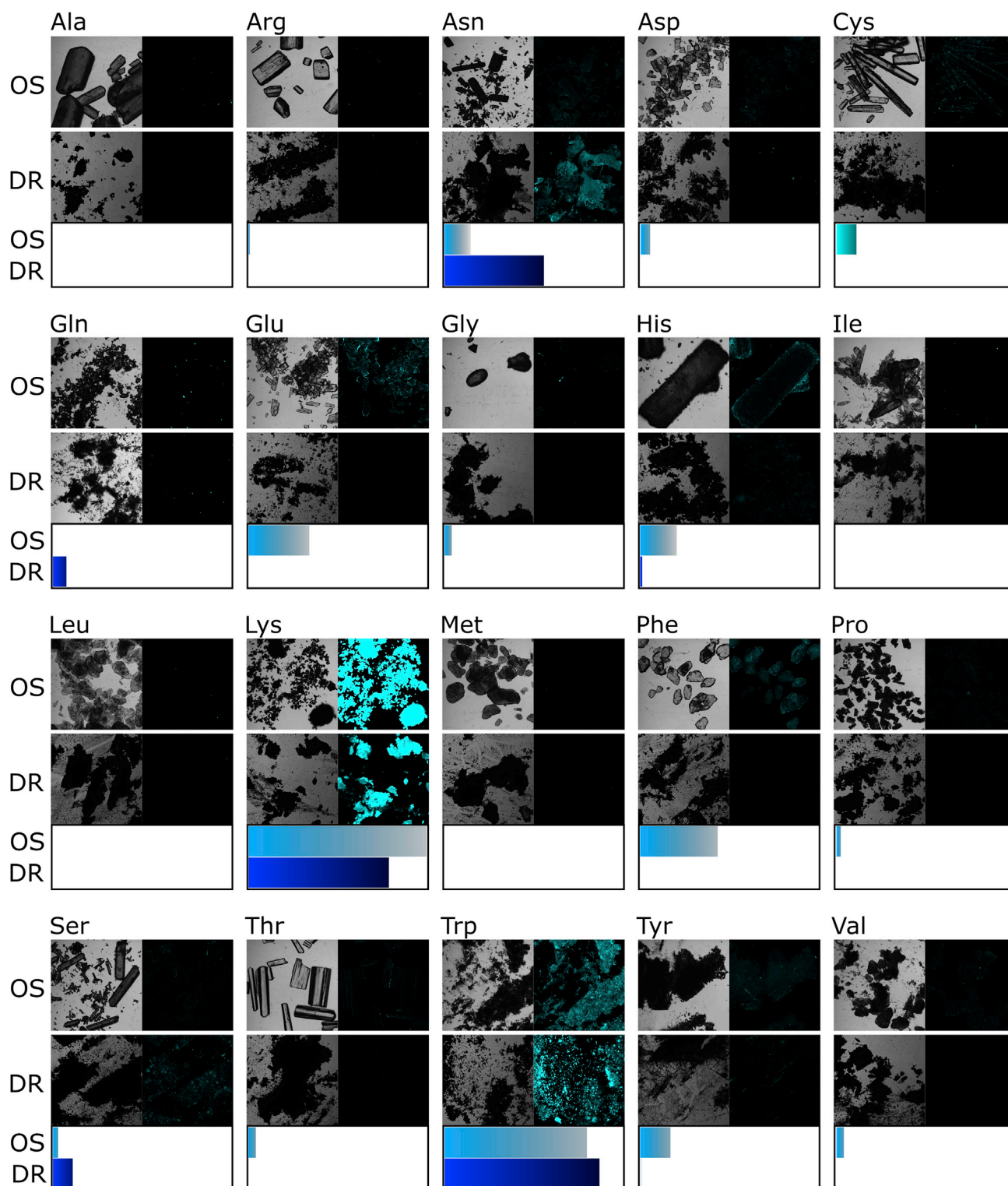


Figure 1. Fluorescence of the 20 coded amino acids

Images of all 20 amino acids, both brightfield (left) and confocal fluorescence at excitation wavelength of 405 nm (right). Amino acid samples as originally obtained from Sigma-Aldrich are displayed in rows marked with OS (Original Sigma). Amino acids dissolved, reassembled, and lyophilized are displayed in

Figure 1. Continued

rows marked with DR (Dissolved and Reassembled). At the bottom of each amino acid panel are the normalized fluorescence signals of the OS sample (light blue) and the DR sample (dark blue).

See also [Tables S1](#) and [S2](#) and [Figure S1](#).

arrangement ([Tikhonova et al., 2018](#)). Indeed, oxidation of aromatic moieties is known to result in the formation of fluorescent products. However, this cannot readily explain the emergence of intrinsic fluorescence upon aggregation of non-aromatic species ([Del Mercato et al., 2007](#); [Jong et al., 2019](#); [Stephens et al., 2020](#)). Overall, the key evidence to distinguish between these options and elucidate the mechanism of intrinsic fluorescence upon aggregation was so far missing. We believe that the reversible transitions between the luminescent and non-luminescent states upon controllable change of aggregate structure is such an evidence. In this work, we aimed at designing and performing such an experiment.

The phenomenon of aggregation-dependent luminescence of proteins is a rapidly evolving field ([Ardona et al., 2017](#); [Arnon et al., 2019](#); [Babar and Sarkar, 2017](#); [Banerjee et al., 2020](#); [Berger et al., 2015](#); [Bhattacharya et al., 2017](#); [Chan et al., 2013](#); [Kong et al., 2019](#); [Niyangoda et al., 2017](#); [Pansieri et al., 2019](#); [Pinotsi et al., 2013, 2016](#); [Prasad et al., 2017](#); [Shaham-Niv et al., 2018](#)). Protein aggregates were shown to absorb light at wavelengths above 300 nm and to exhibit a structure-specific fluorescence in the visible range, even in the absence of aromatic amino acids ([Del Mercato et al., 2007](#)). A plausible explanation for this phenomenon is the formation of structure-specific supramolecular fluorophores that are permissive to proton transfer across hydrogen bonds ([Grisanti et al., 2017](#); [Pinotsi et al., 2016](#); [Yamaguchi et al., 2009](#)). Other hypotheses postulate that the fluorescence is associated with electron-hole recombination due to charge transfer between charged amino acids ([Ardona et al., 2017](#); [Kumar et al., 2020](#); [Prasad et al., 2017](#)) or that deep-blue autofluorescence stems from carbonyl double bonds of the protein backbone ([Niyangoda et al., 2017](#)). Following these studies, we have decided to look into the intrinsic optical properties of single amino acid and metabolite assemblies. Indeed, we have shown that adenine, phenylalanine, tyrosine, and tryptophan exhibit autofluorescence in the visible range upon self-assembly ([Shaham-Niv et al., 2018](#)). This allows the detection of metabolite assemblies within living cells, without any use of external dyes that could interfere with the ability to accurately model a given sample ([Buell et al., 2010](#)). Other derivatives of tyrosine were also shown to exhibit luminescence upon aggregation ([Ren et al., 2019](#)). Yet, the underlying mechanism of the autofluorescence of these assemblies is controversial, as in all cases it can be attributed to the aromatic moiety. In addition, the explanation of impurities as the source of fluorescence is still a plausible option. Here, we have endeavored to study the optical properties of all 20 coded amino acids in a systematic, non-biased approach. Each amino acid was optically characterized in two states: the original powder form, as obtained from the commercial supplier, and after being dissolved in heated water and allowed to cool down for recrystallization. Aiming to simplify the process of assembly and in order to eliminate as many factors as possible, we avoided altering solvents, salt concentrations, changing pH, etc. The systematic evaluation of all amino acids, before and after recrystallization, provides mechanistic insights into the broad phenomenon of assembly-dependent intrinsic fluorescence.

RESULTS

First, we examined the optical properties of the crystalline powders of all 20 coded amino acids in the dried powder form. In addition, each powder was dissolved in water at a high concentration ([Table S1](#)). In order to completely dissolve the powders, the aqueous solution was heated to 90 °C and vortexed until a clear, transparent solution was achieved. The amino acid solutions were then cooled down gradually to room temperature and incubated for several days to allow the formation of assemblies within the solution. The samples were then lyophilized to attain a dried powder of the amino acid assemblies. The optical properties of these powders were examined as well.

The brightfield and confocal fluorescence images obtained under excitation of 405 nm for all 20 amino acids, as originally received (OS, original Sigma) and after dissolution and reassembly (DR, dissolved and reassembled), as well as quantification of the fluorescence signals, are displayed in [Figure 1](#) (see [Figure S1](#) for spectra). For all samples, similar excitation and detection parameters were used. Based on the current measurements there is no systematic trend between the optical properties and the polarity of the amino acids. However, it does appear as though the charged amino acids tend to be characterized by stronger fluorescence, whereas those amino acids with hydrocarbon side chains with methyl groups tend to exhibit very weak optical activity.

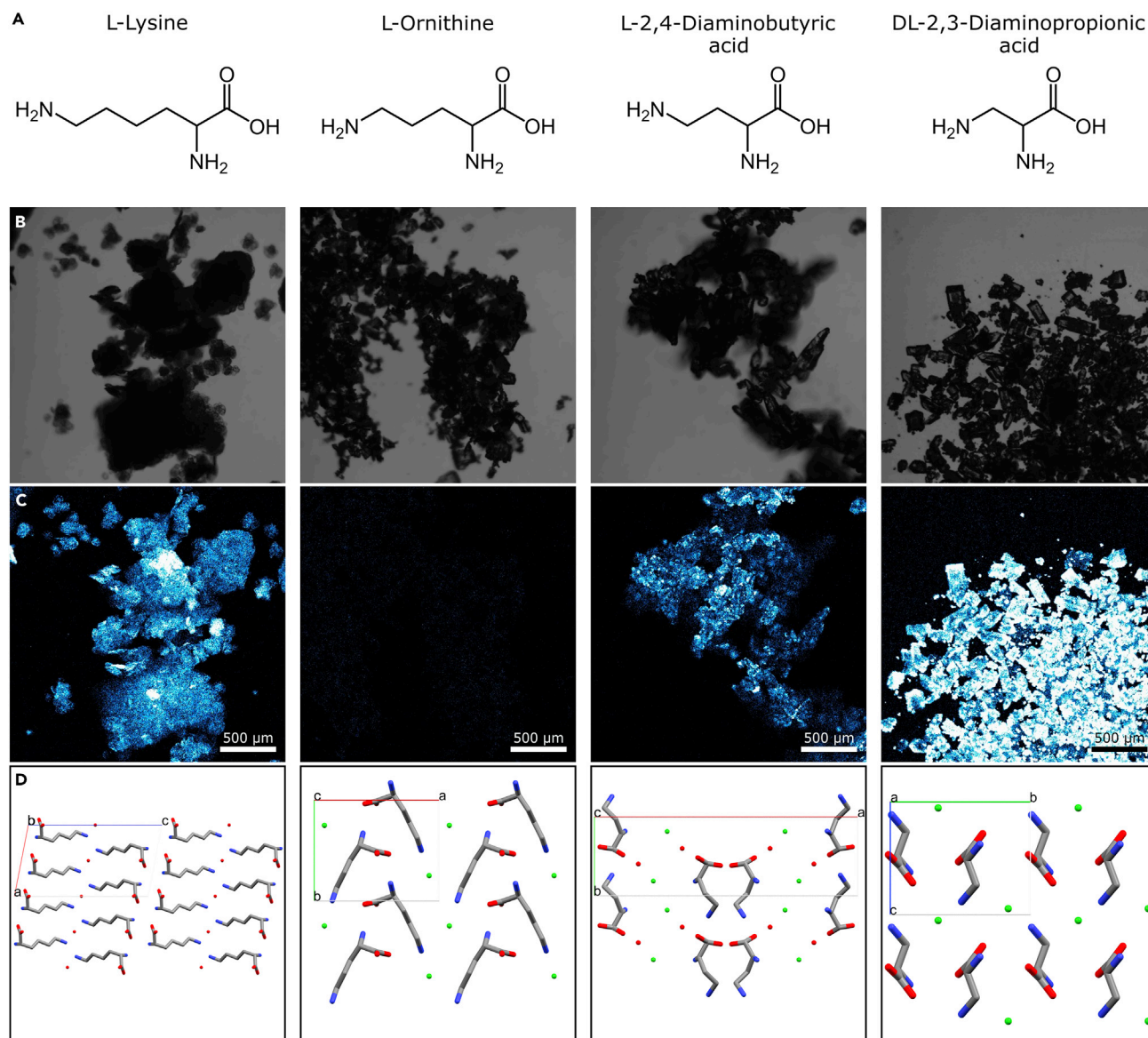


Figure 2. Fluorescence of lysine and its derivatives

(A) The chemical scheme of lysine and its derivatives comprising shorter carbon chains.

(B and C) Microscopy images showing (B) brightfield and (C) fluorescence (excitation at 405 nm) analyses of the four powders. Pixel color represents the intensity; black, non; blue, dim; white, strong.

(D) Crystalline structures of lysine and its derivatives as determined using PXRD.

See also [Data S1](#) for additional crystallographic information.

We then explored the intense fluorescence of L-lysine, which exhibited the brightest signal of all 20 amino acids. We first inquired whether the length of the amine residue chain of lysine, which has four carbons, plays a role in the optical properties of the crystal. For this purpose, we explored the fluorescence of three additional molecules derived from lysine: L-ornithine, L-2,4-diaminobutyric acid, and DL-2,3-diaminopropionic acid, which comprise 3, 2, and 1 side chain carbons, respectively ([Figure 2A](#)). The rationale of this experiment was to alter the crystal packing by shortening the amine residue, thereby modulating the electronic interactions by varying the distance between molecules, and to examine any effect on the resulting optical properties.

All four samples (including lysine) comprised small crystalline powders ([Figure 2B](#)). The fluorescent signal from each sample was obtained using confocal microscopy, similar to the amino acids shown in [Figure 1](#).

Intense fluorescent signals were prominent in the molecules comprising 1-, 2-, and 4-carbon chains, whereas in the 3-carbon chain molecule, ornithine, no visible signal was detected (Figure 2C). The powder X-ray diffraction (PXRD) patterns of the samples were further examined in order to understand the molecular arrangement of the crystals, which might provide insight into the favorable interactions allowing the crystal fluorescence (Figure 2D). The crystal structures of lysine, ornithine, and diaminopropionic acid were previously published (Chiba et al., 1967; Marčeková et al., 2019; Williams et al., 2016). The crystal structure of diaminobutyric acid was determined by the PXRD pattern obtained in this study CCDC Deposition # 1990651 (see STAR Methods). The results revealed the crystal packing of all four samples, allowing molecular inspection of the optical phenomenon. A possible explanation lies in the type of hydrogen bond network that is formed within the supramolecular structure. The NH_2 group of lysine hemihydrate and diaminobutyric acid, and the NH_3^+ of diaminopropionic acid, may interact with a water or chloride ions and donate hydrogen bonds to the molecule complexed in the supramolecular structure. On the other hand, in the case of ornithine, the NH_2 groups do not form hydrogen bonds that are donated from the amine group to either a chloride ion or a water molecule in the complex. Thus, the differences in the supramolecular packing involving the lysine side chains, chloride ions, and water molecules can lead to differences in the optical properties. We believe that the packing of the crystal is an important factor in determining its optical behavior, much like the properties of microenvironments such as different solvents, ionic strength, polarity, or molecular concentration could be significant for structure-function attributes.

Following this line of evidence, we focused on possible interconnections between the optical and structural properties of amino acid powders.

Next, each of the 20 amino acid samples was examined using PXRD to determine the crystalline structure. The results are summarized in Table S2. Most amino acid crystals were composed of the same crystal structure in both the OS and the DR samples. Of the 20 amino acids, only cysteine and serine displayed different powder diffraction between their respective OS and DR samples, with a single crystal packing observed in each sample. However, both serine samples exhibited some level of fluorescence, whereas the cysteine DR sample did not show any detectable fluorescence (Figure 1), making the differentiation between the cysteine samples much more straightforward. In addition, the DR serine sample was found to comprise a hemihydrate crystal packing (Table S2), adding another factor of complexity, while both cysteine crystals showed different arrangements of cysteine alone, with four molecules in both unit cells. Hence, we further investigated the OS and DR samples of cysteine (Figures 3A and 3B), which showed a clear difference in the fluorescent signal (Figure 3C) and exhibited an orthorhombic and monoclinic packing, respectively (Figures 3D and 3E) (Harding and Long, 1968; Kerr and Ashmore, 1973). Since the process of attaining the OS powder is unknown to us, we have decided to crystallize an orthorhombic cysteine crystal after dissolving the amino acid in order to control the entire procedure. We were able to crystallize both crystal packings, orthorhombic and monoclinic, depending on the crystallization temperature, 4 °C and 25 °C, respectively, as the only difference in the crystallization conditions. This allowed a reversible crystallization of both crystal packings, exemplifying the significance of the crystal packing to the optical properties of the crystal. Thus, the fluorescent OS powder (Figure 3F) was dissolved and recrystallized at 25 °C to obtain the non-fluorescent monoclinic DR sample (Figure 3G) and then re-dissolved and recrystallized at 4 °C to form yet again the fluorescent orthorhombic crystals (Figure 3H). To confirm that the fluorescence does not stem from impurities, the non-fluorescent DR sample was washed several times to remove any impurities that may reside in the supernatant, before recrystallizing as orthorhombic crystals. Although the fluorescent signal of cysteine is relatively low, a difference in the fluorescent signal between the two crystal packings is clearly evident. A comparison of the two structures shows that there is a subtle difference in the proximity of the S-H bonds relative to each other. In the orthorhombic structure, the sulfide groups are packed closer to each other and may facilitate charge transfer, as seen in previous studies (Del Mercato et al., 2007; Pinotsi et al., 2016; Prasad et al., 2017). It is important to note that the overall macroscopic morphology is dictated by other factors in addition to the packing, as evidenced by different morphologies for an identical packing (compare Figures 3F–3H), and vice versa (compare Figures 3G–3H). For this reason, the crystal packing was determined using PXRD for each sample and for every iteration. Morphologically, the recrystallized orthorhombic structures (Figure 3H) are similar to the non-fluorescent monoclinic structures (Figure 3G) and are dissimilar to the relatively large OS crystals (Figure 3F); hence, this affirms that the difference in fluorescence is not derived from any morphological discrepancy. As stated above, the crucial experiment to prove the influence of crystal packing on intrinsic fluorescent formation could be an observation of reversible transitions between the luminescent and non-luminescent states upon controllable

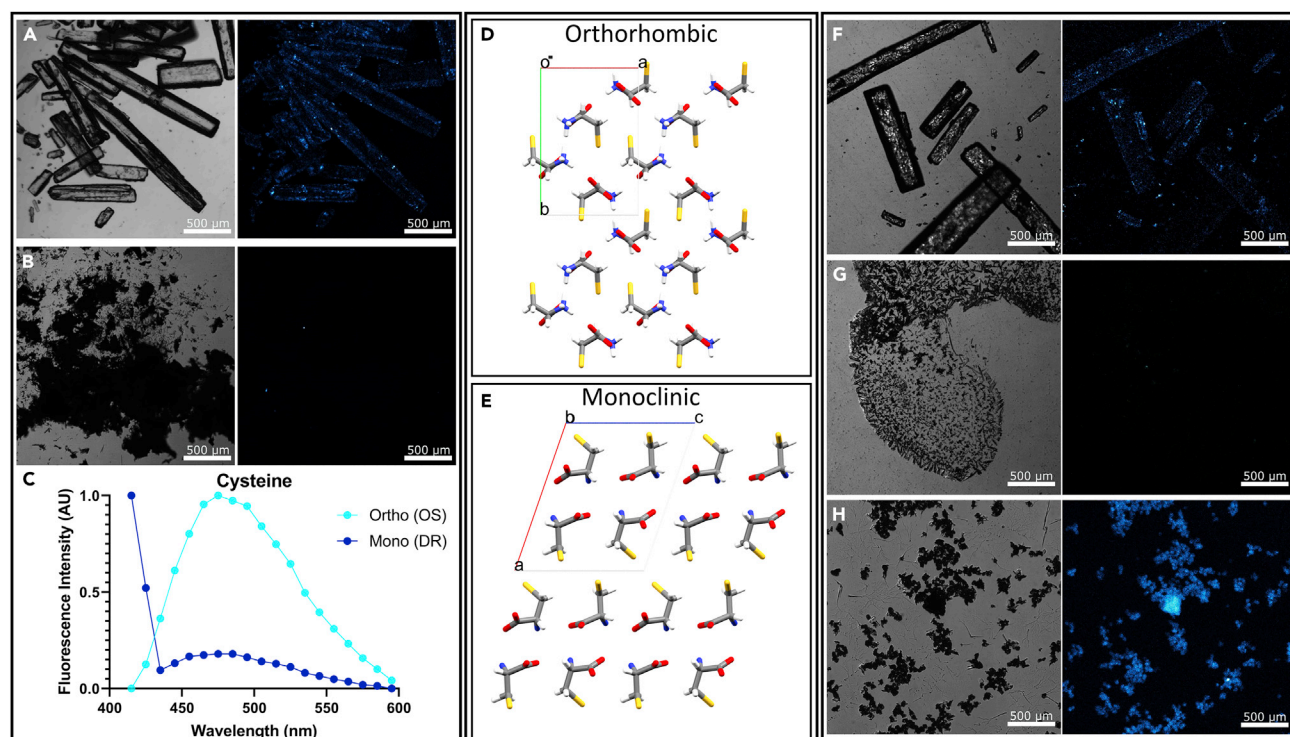


Figure 3. Fluorescence of cysteine

For a Figure360 author presentation of Figure 3, see <https://doi.org/10.1016/j.isci.2021.102695>.

(A and B) Confocal microscopy images of the cysteine (A) OS sample and (B) DR sample.

(C) The normalized fluorescence intensity of cysteine samples as a function of the emission wavelength (excitation at 405 nm).

(D and E) Crystalline structures of cysteine based on PXRD analysis showing (D) the orthorhombic packing of the OS sample and (E) the monoclinic packing of the DR sample.

(F–H) Confocal imaging of the cysteine (F) OS sample, (G) DR sample, and (H) DR sample that was re-dissolved and recrystallized at different conditions to regain an orthorhombic packing. For confocal images, pixel color represents the intensity; black, non; blue, dim; white, strong.

See also Table S3 and Figure S2.

change of the crystal structure. We believe that the observed on-off switching of cysteine fluorescence upon changing its crystal packing (Figure 3) represents such an experiment.

In an attempt to explain the underlying mechanism of the self-assembly-induced fluorescence of amino acids, we tried to find a common thread in the aggregation-induced fluorescence related literature. First principles quantum chemistry calculations of self-assembly-induced fluorescence mainly deal with absorption spectra (Grisanti et al., 2017; Pinotsi et al., 2016; Stephens et al., 2020). Without novel absorption bands, no novel fluorescence bands may appear, and the key to the explanation of the presence of new emission properties is the understanding of long-wavelength absorption formation. This paradigm was extended in the recent work of Grisanti et al., where, using *ab initio* calculations, fluorescence properties of model peptides aggregates were assessed (Grisanti et al., 2020). Besides the prediction of the emission in the visible spectral range, a conclusion was made on the time-resolved behavior of the aggregation-induced fluorescence. Namely, the presence of an ultrafast fluorescence decay and accompanying spectral diffusion, i.e., a gradual fluorescence emission redshift in time, on a sub-picosecond timescale, was described theoretically. This result prompted us to search for experimental indication of an ultrafast component in a self-assembly-induced fluorescence system by means of the ultrafast spectroscopy. Taking into account the universal character of this emission, i.e., similarity of its spectral properties for a broad range of systems, we chose to work with a known model system—fibrillar structures that are formed as a result of phenylalanine self-assembly. The fluorescence of phenylalanine was previously characterized, and showed high fluorescent signal, much higher than the unfortunately too weak signal of cysteine, which was insufficient for these measurements (Shaham-Niv et al., 2018). Thus, by the example of the fibrils made of phenylalanine, we aim at corroborating the presence of an ultrafast fluorescence decay of the self-assembly-induced fluorescence.

The self-assembly of phenylalanine in aqueous solution was initiated by cooling a supersaturated solution of phenylalanine (40 mg/ml) at 90 °C to 20 °C, similar to previous work (Shaham-Niv et al., 2018). This leads to the formation of elongated fibrillary aggregates, as shown by bright-field microscopy (Figure 4A). The phenylalanine fibrils exhibited relatively high fluorescence emission in the visible spectral range, which is absent in the monomeric state of phenylalanine, and were characterized by the wavelength-dependent Stokes shift, i.e., the spectra measured at longer excitation wavelength exhibited red-shifted emission (Figure 4B). Such a behavior of the fluorescence emission band is known as the red-edge excitation shift effect and is characteristic for the self-assembly-induced fluorescence of amino acids, peptides, and proteins (Arnon et al., 2019; Berger et al., 2015; Kumar et al., 2020). The presence of elongated fibrillar structures was detectable by fluorescence lifetime imaging, without the use of any external dyes, only by using the autofluorescence signal of the sample (Figure 4C). The autofluorescence decay curve obtained for the phenylalanine fibrils revealed the presence of 0.35- and 2.53-ns decay times after fitting to a biexponential model (Figure 4D). However, the temporal resolution, or the width of the instrument response function (IRF) of the fluorescence lifetime imaging setup, which employs the standard time-correlated single photon counting technique, is ~50 ps and does not allow for detecting any ultrafast decay components, which will be completely masked by the 50-ps IRF (Rovnyagina et al, 2019, 2020). Hence, we have utilized the fluorescence up-conversion technique, which provides for sub-picosecond resolution of fluorescence decay (for more information, see STAR Methods).

Using fluorescence up-conversion, it was observed that the phenylalanine fibrils exhibited ultrafast decay lifetime component as fast as 0.67 ps (Figure 4E). The second decay component was characterized by a 12.6 ps decay. The presence of the sub-picosecond fluorescence decay is in agreement with the calculation of the recent published work (Grisanti et al., 2020), where the spectral diffusion and relaxation was observed on a few hundred picoseconds timescale.

In the work of Grisanti et al., the *ab initio* nonadiabatic dynamics simulations were used to reveal characteristic properties of the excited electronic states of model amyloid-like peptides. It was shown that a visible (blue-green) fluorescence could originate from the $n\pi^*$ states localized on the amide groups. The specific structure of amyloids gives rise to stabilization of some of these states, thus lowering the energy gap between the ground and minimum $n\pi^*$ state leading to the shift of absorption and fluorescence to the near UV-visible range. Grisanti and co-workers observed that, after excitation in the manifold of $n\pi^*$ states in 10–15 fs all trajectories from different $n\pi^*$ states reached the lowest excited S_1 (or $n\pi^*_{\min}$, according to Grisanti et al.) state. In the range of 15–40 fs after excitation UV fluorescence from S_1 state is observed and is peaked at 3.3 eV (~370 nm). After that, on the timescale of ~100–200 fs, internal vibration redistribution occurs that leads to additional redshift of the emission spectrum, down to 2.0 eV (620 nm) (Figure 4F).

This evolution occurs on the timescale of ~100 fs and is accompanied by the gradual shift of the fluorescence emission from the UV to the blue-green region (Figure 4G). By setting the registration emission wavelength to the blue-green region (in our case, to 500 nm [~2.5 eV]), the ultrafast relaxation along the potential curve shown in Figure 4F can be detected. This process is illustrated in the inset of Figure 4G and corresponds to the fluorescence decay curve presented in Figure 4E. The ultrafast relaxation occurs on the timescale of ~100 fs, corresponding to the non-radiative decay rate of $\sim 10^{12}$ – 10^{13} s⁻¹, which is, however, lower than in the case of monomeric proteins, where the lack of stabilization of the $n\pi^*$ states results in the absence of near-UV and visible absorption and blue-green fluorescence (Grisanti et al., 2020). Moreover, the presence of the ultrafast decay may result in low fluorescence quantum yield of the aggregation-induced emission of proteins (~0.01) (Niyangoda et al., 2017). Further relaxation from the lowest energy $n\pi^*_{\min}$ state may then occur on a longer timescale owing to the stabilization of the geometry of the aggregate, and this relaxation corresponds to the 1 to 2-ns fluorescence lifetime, which was observed for the self-assembly-induced fluorescence in this paper (Figure 4D) and other previous works (Tikhonova et al., 2018). Hence, by detecting the ultrafast decay of the fibrillar structures formed as the result of phenylalanine self-assembly, the model of Grisanti et al. can be extended from peptides to amino acids, therefore elucidating the origin of their enigmatic fluorescence emission upon packing (Grisanti et al., 2020).

DISCUSSION

To conclude, in this work we have studied the optical properties of all 20 coded amino acid powders. Each powder was examined as commercially obtained and also after dissolution, reassembly, and lyophilization. It is surprising

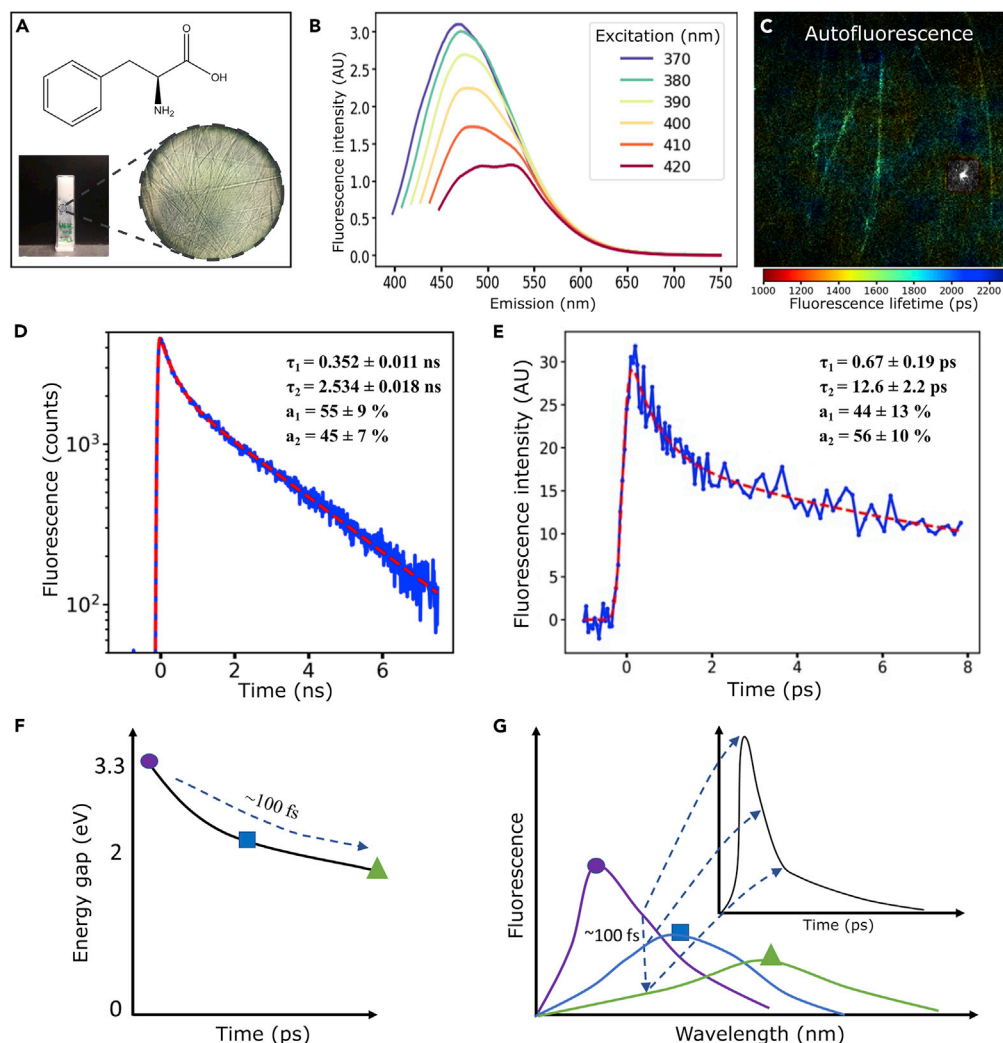


Figure 4. Ultrafast decay

(A) Chemical scheme and fibrils of phenylalanine (macroscopic and microscopic photos).
 (B) Fluorescence emission of phenylalanine assemblies at excitations between 370 and 420 nm.
 (C) Autofluorescence lifetime imaging of phenylalanine fibrils. Excitation was performed in a two-photon regime at 700 nm.
 (D) Fluorescence decay curve of the phenylalanine fibrils measured with (sub)nanosecond resolution.
 (E) Fluorescence decay curve of phenylalanine fibrils measured using fluorescence up-conversion technique. Excitation and emission were set to 380 and 450 nm, respectively. The inset shows the parameters of fluorescence decay obtained using the biexponential decay model (D and E).
 (F) Schematic decrease in the energy gap between the excited $n\pi^*$ and ground state of the model fibrils.
 (G) Scheme of the shift of the aggregation-induced fluorescence spectrum with time, demonstrating the presence of the ultrafast decay and spectral migration.

that lysine exhibited the most intense fluorescence, even though it has no aromatic moieties. Other charged amino acids showed little to no fluorescence. In addition, short-chain derivatives of lysine displayed no correlation between the chain length and their intrinsic fluorescence. This indicates that, in some cases, not only the chemical identity of the monomeric molecule dictates the optical properties of the assembly, but also the supramolecular arrangement within the assembly. To substantiate this notion, PXRD analysis together with confocal imaging revealed that the orthorhombic crystal of cysteine is fluorescent, whereas the monoclinic crystal is not. The recrystallization of the non-fluorescent monoclinic crystals into fluorescent orthorhombic crystals confirms that, in this case, changing the crystal packing is sufficient for conferring optical properties, and that the fluorescence does not stem from contaminations, impurities, or oxidation. It is important to note that we do not imply that impurities,

oxidation, or aromatic interactions are not valid mechanisms that could explain the fluorescence in some cases. However, in addition to those, supramolecular interactions may also affect the optical properties of other biomolecular assemblies, as unambiguously presented here, thus playing a key role in a phenomenon that could be explained by other known mechanisms. In the literature it was proposed that peptide aggregation-induced fluorescence in the blue-green spectral range is due to (1) delocalization of electrons over a network of hydrogen bonds (Shukla et al., 2004), (2) hydrogen bond-mediated interactions between the amide groups (Ye et al., 2017), (3) proton transfer across hydrogen bonds (Pinotsi et al., 2016), and (4) a decrease in the energy gap between the excited and ground states caused by the influence of the hydrogen bonds on the amide group geometry (Ye et al., 2017). The importance and role of the structure for fluorescence formation in aggregates of non-aromatic peptides has been recently addressed using *ab initio* nonadiabatic dynamics simulations of the excited electronic states (Ye et al., 2017). In addition, previous work has shown that low-energy optical excitations and subsequent fluorescence can be induced by charge-transfer excitations (Jong et al., 2019; Mandal et al., 2019; Prasad et al., 2017). Specifically, charge transfer excitations involving sulfur atoms of methionine and the positively charged N termini of amyloid aggregates were presented (Jong et al., 2019). In the case of cysteine demonstrated in this work, the difference in the molecular packing within the crystal alters the distances between the sulfur atom and the N termini of the neighboring molecule, which could affect the charge transfer potential. Indeed, these distances are shorter for the orthorhombic crystal in comparison with the monoclinic packing (Figure S2). Overall, on the basis of previous research, it can be summarized that the chromophore responsible for the aggregation-induced absorption and fluorescence in the visible range is structure specific and can be formed either in the absence or presence of aromatic moieties in peptides. Our results demonstrate that even the simplest and most thoroughly investigated molecular systems, such as amino acids, can still serve as the basis for new, intriguing, and unknown phenomena. The reversibility of cysteine fluorescence serves as a strong evidence that the molecular arrangement has a crucial role in the observed optical properties.

The prediction of ultrafast decay by Grisanti et al. was experimentally confirmed in an aggregation-induced fluorescence model system of phenylalanine fibrils. Specifically, the presence of the ultrafast decay of the blue-green autofluorescence is in agreement with the hypothesis regarding the governing role of amyloid structure-stabilized $n\pi^*$ states in the emission formation. Although the experimental data do not exclude other hypotheses, its relevance to the theoretical calculations can be a step toward understanding the origin of the blue-green emission in amyloids and other systems that recently attracts increased interest, which appear as a result of peptides and amino acid self-assembly. Further understanding of the underlying mechanisms could aid in harnessing the intrinsic properties of supramolecular polymers self-assembled by simple and cost-effective building blocks to develop smart optoelectronic materials.

Limitations of the study

The current study aims to systematically explore, in a non-bias manner, the requirements for autofluorescence upon aggregation. Nevertheless, it is limited only to the 20 coded amino acids. Although we observed similar optical behavior for other small molecules, such as metabolites and nucleotides, further research, beyond the scope of this study, is necessary to understand the fundamental principles of this phenomenon. In addition, there are numerous other questions that could be asked and researched for regarding these systems, such as the effect of racemic amino acids, different solvents, or ionic strength. Questions like what is the “proper packing” for fluorescence? What are the requirements? This is the main enigma. Once we know the answer, we can potentially pre-design the optical properties of a material. Although we did not find a clear-cut answer to this question, we believe that this article is a big step in the right direction.

STAR★METHODS

Detailed methods are provided in the online version of this paper and include the following:

- KEY RESOURCES TABLE
- RESOURCE AVAILABILITY
 - Lead contact
 - Materials availability
 - Data and code availability
- METHOD DETAILS
 - Amino acid reassembly
 - Confocal imaging

- Image analysis
- Powder X-Ray diffraction
- Cysteine crystallization
- Phenylalanine fibrils sample preparation
- Steady-state fluorescence measurements of phenylalanine fibrils
- Fluorescence lifetime microscopy (FLIM)
- Sub-picosecond fluorescence lifetime measurements

SUPPLEMENTAL INFORMATION

Supplemental information can be found online at <https://doi.org/10.1016/j.isci.2021.102695>.

ACKNOWLEDGMENTS

Z.A.A. and T.K. contributed equally to this work. We thank our lab members for the fruitful discussions. This work was supported by the Israeli National Nanotechnology Initiative and Helmsley Charitable Trust (E.G.), the European Research Council BISON project (E.G.), the Clore Scholarship program and the Marian Gertner Institute (Z.A.A.). The work was supported by the Ministry of Science and Higher Education of the Russian Federation within the framework of state support for the creation and development of World-Class Research Centers "Digital biodesign and personalized healthcare" No075-15-2020-926 (E.S.). We thank members of the Gazit group for the helpful discussions.

AUTHOR CONTRIBUTIONS

Z.A.A., T.K., S.S.-N., and E.G. conceived and designed the experiments. Z.A.A., T.K., N.B., R.A., S.S.-N., P.M., M.N.Q., E.P., A.R., I.S., A.H., E.S., and D.L. planned and performed the experiments. Z.A.A., T.K., and E.G. wrote the manuscript. D.L. performed PXRD experiments and analysis. All authors discussed the results, provided intellectual input and critical feedback, and commented on the manuscript.

DECLARATION OF INTERESTS

The authors declare no competing interests.

Received: April 12, 2021

Revised: May 17, 2021

Accepted: June 4, 2021

Published: July 23, 2021

SUPPORTING CITATIONS

The following references appear in the supplemental information: Almlöf et al., 1973; Coll et al., 1986; Derissen et al., 1968; Frey et al., 1973; Janczak and Luger, 1997; Kayushina, 1965; Khawas and Krishna Murti, 1969; King et al., 2012; Kistenmacher et al., 1974; Koetzle et al., 1973; Kwick et al., 1980; Lehmann et al., 1972; Mazumdar et al., 1969; Mostad et al., 1973; Oda and Koyama, 1972; Ramanadham et al., 1973; Torii and Iitaka, 1973; Torii and Iitaka, 1971; Torii and Iitaka, 1970; Verbist et al., 1972; Wilson et al., 2005; Yamada et al., 2007.

REFERENCES

- Almlöf, J., Kwick, Å., and Thomas, J.O. (1973). Hydrogen bond studies. 77. Electron density distribution in α -glycine: X-N difference Fourier synthesis vs ab initio calculations. *J. Chem. Phys.* 59, 3901–3906. <https://doi.org/10.1063/1.1680574>.
- Altomare, A., Cuocci, C., Giovacazzo, C., Moliterni, A., Rizzi, R., Corriero, N., and Falcicchio, A. (2013). EXPO2013: a kit of tools for phasing crystal structures from powder data. *J. Appl. Crystallogr.* 46, 1231–1235. <https://doi.org/10.1107/S0021889813013113>.
- Ardon, H.A.M., Draper, E.R., Citossi, F., Wallace, M., Serpell, L.C., Adams, D.J., and Tovar, J.D. (2017). Kinetically controlled coassembly of multichromophoric peptide hydrogelators and the impacts on energy transport. *J. Am. Chem. Soc.* 139, 8685–8692. <https://doi.org/10.1021/jacs.7b04006>.
- Arnon, Z.A., Berger, O., Aizen, R., Hannes, K., Brown, N., Shimon, L.J.W., and Gazit, E. (2019). Coassembly of complementary peptide nucleic acid into crystalline structures by microfluidics. *Small Methods* 3, 1900179. <https://doi.org/10.1002/smt.201900179>.
- Babar, D.G., and Sarkar, S. (2017). Self-assembled nanotubes from single fluorescent amino acid. *Appl. Nanosci.* 7, 101–107. <https://doi.org/10.1007/s13204-017-0551-5>.
- Banerjee, P., Pyne, A., and Sarkar, N. (2020). Understanding the self-assembling behavior of biological building block molecules: a spectroscopic and microscopic approach. *J. Phys. Chem. B* 124, 2065–2080. <https://doi.org/10.1021/acs.jpcc.9b09123>.
- Berger, O., Adler-Abramovich, L., Levy-Sakin, M., Grunwald, A., Liebes-Peer, Y., Bachar, M., Buzhansky, L., Mossou, E., Forsyth, V.T., Schwartz, T., et al. (2015). Light-emitting self-assembled peptide nucleic acids

exhibit both stacking interactions and Watson-Crick base pairing. *Nat. Nanotechnol.* 10, 353–360. <https://doi.org/10.1038/nnano.2015.27>.

Bhattacharya, A., Bhowmik, S., Singh, A.K., Kodgire, P., Das, A.K., and Mukherjee, T.K. (2017). Direct evidence of intrinsic blue fluorescence from oligomeric interfaces of human serum albumin. *Langmuir* 33, 10606–10615. <https://doi.org/10.1021/acs.langmuir.7b02463>.

Buell, A.K., Dobson, C.M., Knowles, T.P.J., and Welland, M.E. (2010). Interactions between amyloidophilic dyes and their relevance to studies of amyloid inhibitors. *Biophys. J.* 99, 3492–3497. <https://doi.org/10.1016/j.bpj.2010.08.074>.

Chan, F.T.S., Kaminski Schierle, G.S., Kumita, J.R., Bertoncini, C.W., Dobson, C.M., and Kaminski, C.F. (2013). Protein amyloids develop an intrinsic fluorescence signature during aggregation. *Analyst* 138, 2156–2162. <https://doi.org/10.1039/c3an36798c>.

Chen, X., Luo, W., Ma, H., Peng, Q., Yuan, W.Z., and Zhang, Y. (2018). Prevalent intrinsic emission from nonaromatic amino acids and poly(amino acids). *Sci. China Chem.* 61, 351–359. <https://doi.org/10.1007/s11426-017-9114-4>.

Chiba, A., Ueki, T., Ashida, T., Sasada, Y., and Kakudo, M. (1967). The crystal structure of L-ornithine hydrochloride. *Acta Crystallogr.* 22, 863–870. <https://doi.org/10.1107/S0365110X67001690>.

Coll, M., Solans, X., Font-Altaba, M., and Subirana, J.A. (1986). Structure of L-leucine: a redetermination. *Acta Crystallogr. C Cryst. Struct. Commun.* 42, 599–601. <https://doi.org/10.1107/S0108270186095240>.

Del Mercato, L.L., Pompa, P.P., Maruccio, G., Della Torre, A., Sabella, S., Tamburro, A.M., Cingolani, R., and Rinaldi, R. (2007). Charge transport and intrinsic fluorescence in amyloid-like fibrils. *Proc. Natl. Acad. Sci. U S A* 104, 18019–18024. <https://doi.org/10.1073/pnas.0702843104>.

Derissen, J.L., Endeman, H.J., and Peerdeman, A.F. (1968). The crystal and molecular structure of L-aspartic acid. *Acta Crystallogr. B Struct. Crystallogr. Cryst. Chem.* 24, 1349–1354. <https://doi.org/10.1107/S0567740868004280>.

Frey, M.N., Lehmann, M.S., Koetzle, T.F., and Hamilton, W.C. (1973). Precision neutron diffraction structure determination of protein and nucleic acid components. XI. Molecular configuration and hydrogen bonding of serine in the crystalline amino acids L-serine monohydrate and DL-serine. *Acta Crystallogr. B Struct. Crystallogr. Cryst. Chem.* 29, 876–884. <https://doi.org/10.1107/S0567740873003481>.

Grisanti, L., Pinotsi, D., Gebauer, R., Kaminski Schierle, G.S., and Hassanali, A.A. (2017). A computational study on how structure influences the optical properties in model crystal structures of amyloid fibrils. *Phys. Chem. Chem. Phys.* 19, 4030–4040. <https://doi.org/10.1039/c6cp07564a>.

Grisanti, L., Sapunar, M., Hassanali, A., and Doslić, N. (2020). Toward understanding optical properties of amyloids: a reaction path and nonadiabatic dynamics study. *J. Am. Chem. Soc.*

142, 18042–18049. <https://doi.org/10.1021/jacs.0c07134>.

Guerin, S., Stapleton, A., Chovan, D., Mouras, R., Gleeson, M., McKeown, C., Noor, M.R., Silien, C., Rhen, F.M.F.F., Kholkin, A.L.L., et al. (2018). Control of piezoelectricity in amino acids by supramolecular packing. *Nat. Mater.* 17, 180–186. <https://doi.org/10.1038/nmat5045>.

Harding, M.M., and Long, H.A. (1968). The crystal and molecular structure of L-cysteine. *Acta Crystallogr. B Struct. Crystallogr. Cryst. Chem.* 24, 1096–1102. <https://doi.org/10.1107/S0567740868003742>.

Janczak, J., and Luger, P. (1997). L-proline monohydrate at 100 K. *Acta Crystallogr. C Cryst. Struct. Commun.* 53, 1954–1956. <https://doi.org/10.1107/S0108270197011487>.

Ji, W., Xue, B., Arnon, Z.A.Z.A., Yuan, H., Bera, S., Li, Q., Zaguri, D., Reynolds, N.P.N.P., Li, H., Chen, Y., et al. (2019). Rigid tightly packed amino acid crystals as functional supramolecular materials. *ACS Nano* 13, 14477–14485. <https://doi.org/10.1021/acs.nano.9b08217>.

Jong, K.H., Azar, Y.T., Grisanti, L., Stephens, A.D., Jones, S.T.E.E., Credgington, D., Kaminski Schierle, G.S., and Hassanali, A. (2019). Low energy optical excitations as an indicator of structural changes initiated at the termini of amyloid proteins. *Phys. Chem. Chem. Phys.* 21, 23931–23942.

Kayushina, R.L.V.B.R. (1965). Opredepenie strukturi L-prolina. *Kristallografiya* 10, 833–844.

Kerr, K.A., and Ashmore, J.P. (1973). Structure and conformation of orthorhombic L-cysteine. *Acta Crystallogr. B Struct. Crystallogr. Cryst. Chem.* 29, 2124–2127. <https://doi.org/10.1107/S0567740873006217>.

Khawas, B., and Krishna Murti, G.S.R. (1969). On the unit-cell dimensions and space group of L-tyrosine and L-tryptophane. *Acta Crystallogr. B Struct. Crystallogr. Cryst. Chem.* 25, 1006–1009. <https://doi.org/10.1107/S0567740869003426>.

King, M.D., Blanton, T.N., and Korter, T.M. (2012). Revealing the true crystal structure of L-phenylalanine using solid-state density functional theory. *Phys. Chem. Chem. Phys.* 14, 1113–1116. <https://doi.org/10.1039/c1cp22831e>.

Kistenmacher, T.J., Rand, G.A., and Marsh, R.E. (1974). Refinements of the crystal structures of DL-serine and anhydrous L-serine. *Acta Crystallogr. B Struct. Crystallogr. Cryst. Chem.* 30, 2573–2578. <https://doi.org/10.1107/S0567740874007618>.

Koetzle, T.F., Frey, M.N., Lehmann, M.S., and Hamilton, W.C. (1973). Precision neutron diffraction structure determination of protein and nucleic acid components. XIII. Molecular and crystal structure of the amino acid L-glutamine. *Acta Crystallogr. B Struct. Crystallogr. Cryst. Chem.* 29, 2571–2575. <https://doi.org/10.1107/S0567740873007028>.

Kong, J., Wang, Y., Qi, W., Su, R., and He, Z. (2019). Photo- and aromatic stacking-induced green emissive peptidyl nanoparticles for cell imaging and monitoring of nucleic acid delivery. *ACS Appl. Mater. Interfaces* 11, 15401–15410. <https://doi.org/10.1021/acsami.9b03945>.

Kumar, A., Ahari, D., Priyadarshi, A., Ziauddin Ansari, M., and Swaminathan, R. (2020). Weak intrinsic luminescence in monomeric proteins arising from charge recombination. *J. Phys. Chem. B* 124, 2731–2746. <https://doi.org/10.1021/acs.jpcc.9b10071>.

Kvick, Å., Canning, W.M., Koetzle, T.F., and Williams, G.J.B. (1980). An experimental study of the influence of temperature on a hydrogen-bonded system: the crystal structure of γ -glycine at 83 K and 298 K by neutron diffraction. *Acta Crystallogr. B Struct. Crystallogr. Cryst. Chem.* 36, 115–120. <https://doi.org/10.1107/S0567740880002555>.

Lakowicz, J.R., Shen, B., Gryczynski, Z., D'Auria, S., and Gryczynski, I. (2001). Intrinsic fluorescence from DNA can be enhanced by metallic particles. *Biochem. Biophys. Res. Commun.* 286, 875–879. <https://doi.org/10.1006/bbrc.2001.5445>.

Lehmann, M.S., Koetzle, T.F., and Hamilton, W.C. (1972). Precision neutron diffraction structure determination of protein and nucleic acid components. VIII: the crystal and molecular structure of the β -form of the amino acid L-glutamic acid. *J. Cryst. Mol. Struct.* 2, 225–233. <https://doi.org/10.1007/BF01246639>.

Makam, P., Yamijala, S.S.R.K.C., Tao, K., Shimon, L.J.W., Eisenberg, D.S., Sawaya, M.R., Wong, B.M., and Gazit, E. (2019). Non-proteinaceous hydrolase comprised of a phenylalanine metallo-supramolecular amyloid-like structure. *Nat. Catal.* 2, 977–985. <https://doi.org/10.1038/s41929-019-0348-x>.

Mandal, I., Manna, S., and Venkatramani, R. (2019). UV-Visible lysine–glutamate dimer excitations in protein charge transfer spectra: TDDFT descriptions using an optimally tuned CAM-B3LYP functional. *J. Phys. Chem. B* 123, 10967–10979. <https://doi.org/10.1021/acs.jpcc.9b07827>.

Marčeková, M., Gerža, P., Šoral, M., Moncol, J., Berkeš, D., Kolarović, A., and Jakubec, P. (2019). Crystallization does it all: an alternative strategy for stereoselective aza-henry reaction. *Org. Lett.* 21, 4580–4584. <https://doi.org/10.1021/acs.orglett.9b01489>.

Mazumdar, S.K., Venkatesan, K., Mez, H.-C., and Donohue, J. (1969). The crystal structure of L-arginine hydrochloride. *Z. für Krist.* 130, 328–339. <https://doi.org/10.1524/zkri.1969.130.1-6.328>.

Mostad, A., Rømming, C., Graver, H., Husebye, S., Klæboe, P., and Swahn, C.-G. (1973). Crystal structure of DL-tyrosine. *Acta Chem. Scand.* 27, 401–410. <https://doi.org/10.3891/acta.chem.scand.27-0401>.

Niyagoda, C., Miti, T., Breydo, L., Uversky, V., and Muschol, M. (2017). Carbonyl-based blue autofluorescence of proteins and amino acids. *PLoS One* 12, e0176983. <https://doi.org/10.1371/journal.pone.0176983>.

Oda, K., and Koyama, H. (1972). A refinement of the crystal structure of histidine hydrochloride monohydrate. *Acta Crystallogr. B* 28, 639–642. <https://doi.org/10.1107/S0567740872002894>.

Pansieri, J., Jossierand, V., Lee, S.J., Rongier, A., Imbert, D., Sallanon, M.M., Kövari, E., Dane, T.G., Vendrely, C., Chaix-Pluchery, O., et al. (2019). Ultraviolet-visible-near-infrared optical

properties of amyloid fibrils shed light on amyloidogenesis. *Nat. Photon.* 13, 473–479. <https://doi.org/10.1038/s41566-019-0422-6>.

Pinotsi, D., Buell, A.K., Dobson, C.M., Kaminski Schierle, G.S., and Kaminski, C.F. (2013). A label-free, quantitative assay of amyloid fibril growth based on intrinsic fluorescence. *Chembiochem* 14, 846–850. <https://doi.org/10.1002/cbic.201300103>.

Pinotsi, D., Grisanti, L., Mahou, P., Gebauer, R., Kaminski, C.F., Hassanali, A., and Kaminski Schierle, G.S. (2016). Proton transfer and structure-specific fluorescence in hydrogen bond-rich protein structures. *J. Am. Chem. Soc.* 138, 3046–3057. <https://doi.org/10.1021/jacs.5b11012>.

Prasad, S., Mandal, I., Singh, S., Paul, A., Mandal, B., Venkatramani, R., and Swaminathan, R. (2017). Near UV-Visible electronic absorption originating from charged amino acids in a monomeric protein. *Chem. Sci.* 8, 5416–5433.

Ramanadham, M., Sikka, S.K., and Chidambaram, R. (1973). Structure determination of Ls-threonine by neutron diffraction. *Pramana* 1, 247–259. <https://doi.org/10.1007/BF02848502>.

Ren, X., Zou, Q., Yuan, C., Chang, R., Xing, R., and Yan, X. (2019). The dominant role of oxygen in modulating the chemical evolution pathways of tyrosine in peptides: dityrosine or melanin. *Angew. Chem. Int. Ed. Engl.* 58, 5872–5876. <https://doi.org/10.1002/anie.201814575>.

Rovnyagina, N.R., Budylin, G.S., Vainer, Y.G., Tikhonova, T.N., Vasin, S.L., Yakovlev, A.A., Kompanets, V.O., Chekalin, S.V., Priezzhev, A.V., and Shirshin, E.A. (2020). Fluorescence lifetime and intensity of thioflavin T as reporters of different fibrillation stages: insights obtained from fluorescence up-conversion and particle size distribution measurements. *Int. J. Mol. Sci.* 21, 1–16. <https://doi.org/10.3390/ijms21176169>.

Rovnyagina, N.R., Tikhonova, T.N., Kompanets, V.O., Sluchanko, N.N., Tugaeva, K.V., Chekalin, S.V., Fadeev, V.V., Lademann, J., Darvin, M.E., and Shirshin, E.A. (2019). Free and bound Thioflavin T molecules with ultrafast relaxation: implications for assessment of protein binding and aggregation. *Laser Phys. Lett.* 16, 075601. <https://doi.org/10.1088/1612-202X/ab2244>.

Shaham-Niv, S., Arnon, Z.A., Sade, D., Lichtenstein, A., Shirshin, E.A., Kolusheva, S., and Gazit, E. (2018). Intrinsic fluorescence of metabolite amyloids allows label-free monitoring of their formation and dynamics in live cells. *Angew. Chem. Int. Ed. Engl.* 57, 12444–12447. <https://doi.org/10.1002/anie.201806565>.

Shukla, A., Mukherjee, S., Sharma, S., Agrawal, V., Radha Kishan, K., Guptasarma, P., Kishan, K.V.R., and Guptasarma, P. (2004). A novel UV laser-induced visible blue radiation from protein crystals and aggregates: scattering artifacts or fluorescence transitions of peptide electrons delocalized through hydrogen bonding? *Arch. Biochem. Biophys.* 428, 144–153.

Stephens, A.D., Qaisrani, M.N., Ruggiero, M.T., Jones, S.T.E., Poli, E., Bond, A.D., Woodhams, P.J., Kleist, E.M., Grisanti, L., Gebauer, R., et al. (2020). Intrinsic Fluorescence in Non-aromatic Peptide Structures Is Induced by Collective Vibrations, Charge Reorganisation and Short Hydrogen Bonds, as Shown in a New Glutamine-Related Structure (bioRxiv). <https://doi.org/10.1101/2020.01.22.915306>.

Tikhonova, T.N., Rovnyagina, N.R., Zherebker, A.Y., Sluchanko, N.N., Rubekina, A.A., Orekhov, A.S., Nikolaev, E.N., Fadeev, V.V., Uversky, V.N., and Shirshin, E.A. (2018). Dissection of the deep-blue autofluorescence changes accompanying amyloid fibrillation. *Arch. Biochem. Biophys.* 651, 13–20. <https://doi.org/10.1016/j.abb.2018.05.019>.

Toby, B.H., and Von Dreele, R.B. (2013). GSAS-II: the genesis of a modern open-source all purpose crystallography software package. *J. Appl. Crystallogr.* 46, 544–549. <https://doi.org/10.1107/S0021889813003531>.

Torii, K., and Iitaka, Y. (1973). Crystal structures and molecular conformations of L-methionine and L-norleucine. *Acta Crystallogr. B Struct. Crystallogr. Cryst. Chem.* 29, 2799–2807. <https://doi.org/10.1107/S0567740873007569>.

Torii, K., and Iitaka, Y. (1971). The crystal structure of L-isoleucine. *Acta Crystallogr. B Struct. Crystallogr. Cryst. Chem.* 27, 1317–1326. <https://doi.org/10.1107/S0567740871005612>.

Torii, K., and Iitaka, Y. (1970). The crystal structure of L-valine. *Acta Crystallogr. B* 26, 1317–1326. <https://doi.org/10.1107/S0567740870004065>.

Verbist, J.J., Lehmann, M.S., Koetzle, T.F., and Hamilton, W.C. (1972). Precision neutron diffraction structure determination of protein and nucleic acid components. VI. The crystal and molecular structure of the amino acid L-asparagine monohydrate. *Acta Crystallogr. B Struct. Crystallogr. Cryst. Chem.* 28, 3006–3013. <https://doi.org/10.1107/S0567740872007368>.

Williams, P.A., Hughes, C.E., Martin, J., Courvoisier, E., Buanz, A.B.M., Gaisford, S., and Harris, K.D.M. (2016). Understanding the solid-state hydration behavior of a common amino acid: identification, structural characterization, and hydration/dehydration processes of new hydrate phases of L-lysine. *J. Phys. Chem. C* 120, 9385–9392. <https://doi.org/10.1021/acs.jpcc.5b12420>.

Wilson, C.C., Myles, D., Ghosh, M., Johnson, L.N., and Wang, W. (2005). Neutron diffraction investigations of L- and D-alanine at different temperatures: the search for structural evidence for parity violation. *New J. Chem.* 29, 1318. <https://doi.org/10.1039/b419295h>.

Yamada, K., Hashizume, D., Shimizu, T., and Yokoyama, S. (2007). L-Asparagine. *Acta Crystallogr. E Struct. Rep. Online* 63, 3802–3803. <https://doi.org/10.1107/S1600536807039505>.

Yamaguchi, S., Kamikubo, H., Kurihara, K., Kuroki, R., Niimura, N., Shimizu, N., Yamazaki, Y., and Kataoka, M. (2009). Low-barrier hydrogen bond in photoactive yellow protein. *Proc. Natl. Acad. Sci. U S A* 106, 440–444. <https://doi.org/10.1073/pnas.0811882106>.

Ye, R., Liu, Y., Zhang, H., Su, H., Zhang, Y., Xu, L., Hu, R., Kwok, R.T.K., Wong, K.S., Lam, J.W.Y., et al. (2017). Non-conventional fluorescent biogenic and synthetic polymers without aromatic rings. *Polym. Chem.* 8, 1722–1727. <https://doi.org/10.1039/c7py00154a>.

Zou, L., Harkey, M.R., and Henderson, G.L. (2002). Effects of intrinsic fluorescence and quenching on fluorescence-based screening of natural products. *Phytomedicine* 9, 263–267. <https://doi.org/10.1078/0944-7113-00121>.

STAR★METHODS

KEY RESOURCES TABLE

REAGENT or RESOURCE	SOURCE	IDENTIFIER
Chemicals, peptides, and recombinant proteins		
L-Alanine	Sigma-Aldrich	A7627
L-Arginine monohydrochloride	Sigma-Aldrich	11039
L-Asparagine	Sigma-Aldrich	A-0884
L-Aspartic acid	Sigma-Aldrich	A9256
L-Cysteine	Sigma-Aldrich	168179
L-Glutamine	Sigma-Aldrich	G-3126
L-Glutamic acid	Sigma-Aldrich	G1251
L-Glycine	Sigma-Aldrich	G7126
L-Histidine monohydrochloride monohydrate	Sigma-Aldrich	H8125
L-Isoleucine	Sigma-Aldrich	I2752
L-Leucine	Sigma-Aldrich	L8000
L-Lysine	Sigma-Aldrich	L5501
L-Methionine	Sigma-Aldrich	M9625
L-Phenylalanine	Sigma-Aldrich	P2126
L-Proline	Sigma-Aldrich	P-0380
L-Serine	Sigma-Aldrich	S4311
L-Threonine	Sigma-Aldrich	T8625
L-Tryptophan	Sigma-Aldrich	T0254
L-Tyrosine	Sigma-Aldrich	T3754
L-Valine	Sigma-Aldrich	V0500
Deposited data		
Crystal structure of L-2,4-diaminobutyric acid	This Paper; Cambridge Crystallographic Data Center	CCDC: 1990651
Software and algorithms		
GraphPad Prism 9.0.1	GraphPad	https://www.graphpad.com/
ImageJ 1.52	NIH	http://imagej.nih.gov/ij
Inkscape 0.92	Inkscape.org	https://www.inkscape.org
Mercury 4.1.3	Cambridge Crystallographic Data Centre	http://www.ccdc.cam.ac.uk/mercury/
ChemBioDraw Ultra 14.0	PerkinElmer	https://scistore.cambridgesoft.com/chembiodraw/

RESOURCE AVAILABILITY

Lead contact

Further information and requests for resources and materials should be directed to and will be fulfilled by the lead contact, Ehud Gazit (ehudga@tauex.tau.ac.il).

Materials availability

Direct material requests to lead contact, Ehud Gazit.

Data and code availability

The published article includes all datasets generated or analyzed during this study. Crystallographic Information File (CIF) for the crystal structure of L-2,4-diaminobutyric acid can be found in the CCDC database (CCDC Deposition # 1990651).

METHOD DETAILS

Amino acid reassembly

The original samples from Sigma-Aldrich were dissolved in double distilled water, at a relatively high concentration, depending on the water solubility, as detailed in [Table S1](#). The samples were then heated to 90 °C and vortexed to obtain a clear, transparent solution. The solutions were then incubated at room temperature for a week to allow self-assembly and crystallization. The samples were then lyophilized to remove the water and attain a dry crystalline powder.

Confocal imaging

All confocal images were taken using a Leica SP8 Lightning confocal microscope with a Leica Application Suite X (LAS X) software. The samples were excited using a 405 nm laser, with laser intensity set to 50% and the gain set to 500 for all images. The emission range was set between 415 nm to 600 nm. All images were taken at a magnification of 5X.

Image analysis

Images were analyzed using Image J. Since we use confocal microscopy, we can assume that the depth (Z) is very small in comparison to the width and height (X and Y). Thus, in these images we can consider the areas rather than the volumes. For each image, we divided the number of “fluorescent” pixels by the number of “black” pixels in the corresponding brightfield image. The threshold for “fluorescent” and “black” pixels were identical for all the images in each experimental set.

Powder X-Ray diffraction

X-ray diffraction was collected using a Bruker D8 Discover diffractometer with LYNXEYE EX linear position detector. The diffraction pattern to analyze the amino acid structure was performed in a classical θ - θ Bragg-Brentano setup. The diffraction patterns were corroborated based on the reported phases in the PDF-4-organics-2019 database. As the crystal structure of L-2,4-diaminobutyric acid was not reported in the literature, a full crystal structure determination was performed (CCDC Deposition # 1990651; [Data S1](#)). The crystallized powder was placed in a 0.7 mm quartz capillary and a full diffraction pattern was collected between 2 and 50 °, step 0.02 Å. The capillary setup was employed: Göbels mirrors to obtain a parallel beam, rotating capillary holder. The crystallographic structure determination was performed using the EXPO2014 software ([Altomare et al., 2013](#)). These EXPO2014 features used were cell indexing (N-TREOR09 algorithm) and the Simulated Annealing Method.

The solution with the lowest cost function was used as model to perform further crystal refinement on the structure using the GSASII software ([Toby and Von Dreele, 2013](#)). The final error indexes were: wR=10.9% and GoF=3.77.

Cysteine crystallization

Both cysteine crystal packings were crystallized in double distilled water, at an amino acid concentration of 200 mg/ml. Monoclinic packing was attained as described in the “Amino Acid Reassembly” section above. Orthorhombic packing was attained by incubating the solution over night at 4 °C.

Phenylalanine fibrils sample preparation

The sample preparation protocol was analogous to the procedures previously used to create self-assembled phenylalanine -aggregates as previously described ([Shaham-Niv et al., 2018](#)) using the heat-cool technique. Briefly, L-phenylalanine (Panreac Applichem, CAS 63-91-2, no additional purification) in a concentration of 40 mg/ml was dissolved in distilled water (Millipore-Q) at 90 °C (temperature was controlled by the thermostat Qpod 2e, Quantum Northwest, USA) and was stirred for 1 hour using magnetic stirring for complete dissolving. To obtain self-assembled aggregates, the heated phenylalanine solution was cooled to a room temperature of 23-25 °C under normal conditions in cuvettes or on glass slides, depending on the type of the measurement being performed.

Steady-state fluorescence measurements of phenylalanine fibrils

Steady-state fluorescence measurements were performed using the FluoroMax-4 spectrofluorometer (HORIBA Jobin Yvon, Japan). Excitation-emission matrices were measured in the 400-750 nm emission

range with 1 nm step; the excitation wavelength was varied in the 370–420 nm range with a 10 nm step. The spectral widths of the excitation and emission slits were set to 5 nm. The measurements were carried out in a quartz cuvette with an optical path of 1 cm. The measurements were carried out for samples cooled to room temperature.

Fluorescence lifetime microscopy (FLIM)

Fluorescence lifetime imaging microscopy (FLIM) with multiphoton excitation was performed using a custom-build multiphoton multimodal microscopy setup. Femtosecond optical parametric oscillator TOPOL-1050-C (Avesta, Russia), providing excitation by signal wave in the 680–1000 nm range, was used as an excitation source. The pulse width of exciting radiation was ~150 fs, with frequency of 80 MHz, average power at the excitation wavelength on the sample was 1 mW. Scanning over the sample was performed using DSC-120 scan head (Becker&Hickl, Germany). Imaging was performed using oil immersion Plan Apochromat 60× objective with NA=1.4 (CFI Plan Apochromat Lambda 60×, Nikon, Japan). Fluorescence decay curves were detected using hybrid GaAsP detector HPM-100-40 (Becker&Hickl, Germany) with sensitivity in 250–720 nm range and instrument response function characteristic time-width of 120 ps. To cut off the excitation, a 680 nm short-pass dielectric filter was used. Both autofluorescence of phenylalanine-fibers and the thioflavin T fluorescence signals were excited at 730 nm.

Fluorescence decay curves were fitted using SPCImage 8.3 software (Becker&Hickl, Germany) after spatial binning (bin size was equal to 5 for ThT-fluorescence measurements and 10 for autofluorescence measurements) by bi-exponential decay law with respect to instrument response function. Average fluorescence lifetime was calculated as $\tau_m = (a_1 \tau_1 + a_2 \tau_2)/(a_1 + a_2)$, where a_1 , a_2 , τ_1 , τ_2 are the amplitudes and lifetimes obtained from fit.

Sub-picosecond fluorescence lifetime measurements

Time-resolved fluorescence emission measurements in the sub-picosecond time range were carried out using a commercially available femtosecond fluorescence spectrometry system FOG100 (CDP Systems, Russia). The samples were excited by 100 fs pulses at 380 nm with a frequency of 80 MHz (second harmonic of Ti:Sapphire oscillator Mai-Tai, Spectra Physics, USA). The fluorescence signal from the sample was focused on a 0.5 mm β -barium borate crystal alongside the fundamental beam (80 fs, 760 nm), acting as a gate pulse for the frequency up-conversion. The gate pulse was delayed by an automatically controlled delay stage. The upconverted light was focused onto the entrance slit of the double monochromator (spectral resolution < 1.5 nm) and was detected by a photomultiplier tube. The reproducibility of the measurement was checked by 10 times, measuring decay trace. Special rotation cuvette unit was used to avoid photodegradation of the sample.

Similar to steady-state fluorescence and microscopy measurements, a phenylalanine sample in a liquid state, heated to a temperature of 90 °C, was poured into a cuvette and was cooled down to room temperature for 15–20 minutes. The measurements were carried out when the sample was turbid. Fluorescence decay curves were fitted by biexponential decay law with respect to instrument response function fitted as Gaussian function. Data analysis on the sub-picosecond decay curves were performed using custom-built Python scripts using LmFit, Matplotlib, Numpy, Pandas libraries.

[CCDC: 1990651 contains the supplementary crystallographic data for this paper. These data can be obtained free of charge from The Cambridge Crystallographic Data Centre via www.ccdc.cam.ac.uk/data_request/cif.]